Torsion-induced effects in magnetic nanowires

Denis D. Sheka,[1,*] Volodymyr P. Kravchuk,[2,†] Kostiantyn V. Yershov,[2,3,‡] and Yuri Gaididei[2,§]
[1]*Taras Shevchenko National University of Kyiv, 01601 Kyiv, Ukraine*
[2]*Bogolyubov Institute for Theoretical Physics, 03680 Kyiv, Ukraine*
[3]*National University of "Kyiv-Mohyla Academy", 04655 Kyiv, Ukraine*
(Received 19 March 2015; revised manuscript received 21 July 2015; published 10 August 2015)

A magnetic helix wire is one of the simplest magnetic systems which manifests properties of both curvature and torsion. Possible equilibrium magnetization states in the helix wire with different anisotropy directions are studied theoretically. There exist two equilibrium states in the helix wire with easy-tangential anisotropy: a quasitangential magnetization distribution in the case of relatively small curvatures and torsions, and an onion state in the opposite case. The curvature and torsion also essentially influence the spin-wave dynamics in the helix wire, acting as an effective magnetic field. Originated from a geometry-induced effective Dzyaloshinskii interaction, this magnetic field leads to a coupling between the helix chirality and the magnetochirality and breaks mirror symmetry in the spin-wave spectrum: the modification of magnon dispersion relation is linear with respect to the torsion and quadratic with respect to the curvature. All analytical predictions on magnetization statics and dynamics are well confirmed by direct spin-lattice simulations.

DOI: 10.1103/PhysRevB.92.054417 PACS number(s): 75.30.Et, 75.75.−c, 75.78.−n

I. INTRODUCTION

During the past few years, there has been growing interest in the curvature effects in the physics of nanomagnetism. A crucial aspect of the interest is caused by recent achievements in nanotechnologies of flexible, stretchable, and printable magnetoelectronics (see Ref. [1] and references therein). The effects of the curvature on the magnetization structure in nanomagnetic particles of nontrivial geometry were studied for cylinders [2,3], tori [4], half spheres [5], spherical shells [6], hemispherical caps [7,8], cylindrical capped nanomembranes [9], cone shells [10,11], and paraboloidal shells [12]. Chiral and curvature effects taking into account the nonlocal dipolar interaction were discussed for cylinder nanotubes [13–15].

Very recently, we developed a fully three-dimensional (3D) approach for studying statics and dynamics of thin magnetic shells and wires of arbitrary shape [10,11]. This approach gives a possibility to derive the energy for arbitrary curves and surfaces and arbitrary magnetization vector fields on the assumption that the anisotropy contribution greatly exceeds the dipolar and other weak interactions, i.e., for hard magnets. We have shown [11] that due to the curvature, two additional effective magnetic interactions originate from the exchange term: (i) curvature-induced effective anisotropy, which is bilinear with respect to curvature and torsion, and (ii) curvature-induced effective Dzyaloshinskii interaction, which is linear with respect to curvature and torsion. This approach opens doors for studying several perspective directions in nanomagnets, including topologically induced patterns [6,16] and magnetochiral effects [11,16].

The simplest system which displays all the essential features of a 3D curve is a helix with its coordinate-independent curvature and torsion. The interest in such a geometry is motivated also by recent experiments on rolled-up ferromagnetic microhelix coils [17,18]. Depending on the anisotropy direction, different artificial complex helimagnetiklike configurations were experimentally realized: hollow-bar-, corkscrew-, and radial-magnetized 3D microhelix coils [17]. Rolled magnetic structures are now widely discussed in the context of possible application in flexible and stretchable magnetoelectronic devices [19], in particular, rolled-up giant magnetoresistance (GMR) sensors [20], for magnetofluidic applications, spin-wave filters [21,22], and microrobots [23]. Helix coil magnetic structures have a potential to be used in a variety of bioapplication areas, such as in medical procedures, cell biology, or laboratory on a chip [24].

In the current study, our recently developed theory [11] is applied to describe magnetization statics and linear dynamics in the helix wire. We analyze equilibrium states for different types of magnetocrystalline anisotropy. The equilibrium state is determined by the relationship between the curvature, torsion, and the anisotropy strength. We compute phase diagrams of possible equilibrium states for three types of anisotropy (easy tangential, easy normal, and easy binormal) and summarize the results in Fig. 4. In each of these cases, the equilibrium state is either an onion state or an anisotropy-aligned state. For example, in the most interesting case of easy-tangential anisotropy, a quasitangential magnetization distribution appears for strong enough anisotropy; see Figs. 3(a) and 3(b). We show that even in the case of strong anisotropy, the magnetization deviates from the tangent vector. The deviation is determined by the curvature and torsion. There also exists coupling between the helix chirality and the chirality of magnetization distribution (i.e., magnetochirality).

We also study the spin-wave dynamics in the helix wire. Our analysis shows that the curvature and torsion act on magnons in two ways: they cause a standard potential scattering of magnons and they lead to the appearance of an effective magnetic field. The origin of this field is the geometry-induced effective Dzyaloshinskii interaction [11]. Finally, the torsion

*Corresponding author: sheka@univ.net.ua
†vkravchuk@bitp.kiev.ua
‡yershov@bitp.kiev.ua
§ybg@bitp.kiev.ua

breaks the symmetry of the spin-wave spectrum with respect to the direction of the spin-wave propagation; see Fig. 5. This effect is completely analogous to the effect of asymmetry of magnon dispersion due to the natural Dzyaloshinskii interaction in magnetic films [25–27].

The paper is organized as follows. In Sec. II, we introduce a model of a curved magnetic wire and discuss three possible magnetocrystalline anisotropy directions. The model of the helix wire appears in Sec. III. Equilibrium magnetization distributions are described analytically for the easy-tangential helix wire: the quasitangential state (see Sec. III A) and the onion state (see Sec. III B). The phase diagram of energetically preferable states is presented in Sec. III C. The spin-wave dynamics is discussed in Sec. IV. In Sec. V, we study statics and linear dynamics for helix wires with other anisotropy orientations: the easy-normal anisotropy (Sec. V A) and easy-binormal one (Sec. V B). We verify our theory by numerical simulations of the helix-shaped chain of discrete magnetic moments in Sec. VI. In Sec. VII, we present final remarks and discuss possible perspectives and generalizations by paying particular attention to magnetostatic effects. Some details concerning the computation of the onion state are presented in the Appendix.

II. THE MODEL OF A CURVED WIRE

We consider a curved cylindrical wire. Let $\boldsymbol{\gamma}(s)$ be a 1D curve embedded in the 3D space $\mathbb{R}^3$, with s being the arc length coordinate. It is convenient to use the Frenet-Serret reference frame with basic vectors $\boldsymbol{e}_\alpha$:

$$\boldsymbol{e}_\mathrm{T} = \boldsymbol{\gamma}', \quad \boldsymbol{e}_\mathrm{N} = \frac{\boldsymbol{e}_\mathrm{T}'}{|\boldsymbol{e}_\mathrm{T}'|}, \quad \boldsymbol{e}_\mathrm{B} = \boldsymbol{e}_\mathrm{T} \times \boldsymbol{e}_\mathrm{N}, \tag{1}$$

with $\boldsymbol{e}_\mathrm{T}$ being the tangent, $\boldsymbol{e}_\mathrm{N}$ being the normal, and $\boldsymbol{e}_\mathrm{B}$ being the binormal to the curve $\boldsymbol{\gamma}$. Here and below, the prime denotes the derivative with respect to the arc length s and Greek indices α,β enumerate curvilinear coordinates (TNB coordinate) and curvilinear components of vector fields. The relation between $\boldsymbol{e}_\alpha'$ and $\boldsymbol{e}_\alpha$ is determined by Frenet-Serret formulas,

$$\boldsymbol{e}_\alpha' = F_{\alpha\beta}\boldsymbol{e}_\beta, \quad \|F_{\alpha\beta}\| = \begin{Vmatrix} 0 & \kappa & 0 \\ -\kappa & 0 & \tau \\ 0 & -\tau & 0 \end{Vmatrix}.$$

Here, κ and τ are the curvature and torsion of the wire, respectively.

The wire of a finite thickness h can be defined as the following space domain:

$$\boldsymbol{r}(s,u,v) = \boldsymbol{\gamma}(s) + u\boldsymbol{e}_\mathrm{N} + v\boldsymbol{e}_\mathrm{B},$$

where u and v are coordinates within the wire cross section ($|u|,|v| \lesssim h$).

Let us describe the magnetic properties of the wire. The magnetic energy of the wire can collect different contributions such as exchange-interaction energy, magnetocrystalline anisotropy energy, and dipolar (i.e., magnetostatic) interaction. We start our analysis with the case of a so-called *hard* magnet where the anisotropy contribution greatly exceeds the dipolar and other weak interactions. For such hard magnets, a quality factor [28],

$$Q \equiv \frac{K}{2\pi M_s^2}, \tag{2}$$

is supposed to be large; here, $K > 0$ is the constant of magnetocrystalline anisotropy and M_s is the saturation magnetization.

We assume the magnetization spatial one-dimensionality, which can be formalized as $\boldsymbol{m} = \boldsymbol{m}(s,t)$. This assumption is appropriate for the cases when the thickness h does not exceed the characteristic magnetic length $w = \sqrt{\mathcal{A}/K}$, with $\mathcal{A}$ being an exchange constant. The wire thickness is also supposed to be small in comparison with the radii of curvature and torsion. Therefore, our model provides an adequate picture under the following assumptions:

$$h \lesssim w \ll \frac{1}{\kappa}, \frac{1}{\tau}, \quad Q \gg 1. \tag{3}$$

That is why in the current study we can restrict ourselves to the consideration of Heisenberg magnets with the energy

$$E = \mathcal{A}S \int ds(\mathscr{E}_\mathrm{ex} + \mathscr{E}_\mathrm{an}),$$
$$\mathscr{E}_\mathrm{ex} = -\boldsymbol{m}\cdot\nabla^2\boldsymbol{m}, \quad \mathscr{E}_\mathrm{an} = -\frac{(\boldsymbol{m}\cdot\boldsymbol{e}_\mathrm{an})^2}{w^2}, \tag{4}$$

where the unit vector $\boldsymbol{e}_\mathrm{an}$ gives the direction of the anisotropy axis and S is the cross-section area.

Typically, the orientation of the anisotropy axis $\boldsymbol{e}_\mathrm{an}$ is determined by the wire geometry (e.g., it can be tangential to the wire [17]). This means that due to curvilinearity of the wire, it may complicatedly depend on spatial coordinates. Therefore, it is convenient to represent the energy of the magnet in the curvilinear reference frame (1), where $\mathscr{E}_\mathrm{an}$ has the simplest form. For a thin wire, the exchange energy density can be presented as follows [11]:

$$\mathscr{E}_\mathrm{ex} = \mathscr{E}_\mathrm{ex}^0 + \mathscr{E}_\mathrm{ex}^\mathrm{A} + \mathscr{E}_\mathrm{ex}^\mathrm{D}, \quad \mathscr{E}_\mathrm{ex}^0 = |\boldsymbol{m}'|^2,$$
$$\mathscr{E}_\mathrm{ex}^\mathrm{A} = K_{\alpha\beta}m_\alpha m_\beta, \quad \mathscr{E}_\mathrm{ex}^\mathrm{D} = F_{\alpha\beta}(m_\alpha m_\beta' - m_\alpha' m_\beta). \tag{5}$$

Here the first term $\mathscr{E}_\mathrm{ex}^0$ describes a usual isotropic part of the exchange interaction which has the same form as for the straight wire. The second term $\mathscr{E}_\mathrm{ex}^\mathrm{A}$ describes an effective anisotropy interaction, where the components of the tensor $K_{\alpha\beta} = F_{\alpha\nu}F_{\beta\nu}$ are bilinear with respect to the curvature κ and the torsion τ. This term is similar to the "geometrical potential" [29]. (Note that a curvature caused "geometric" effective magnetic field was considered recently for curved magnonic waveguides [30].) The last term $\mathscr{E}_\mathrm{ex}^\mathrm{D}$ in the exchange energy functional is the geometry-induced effective Dzyaloshinskii interaction, which is linear with respect to curvature and torsion. As shown below, this interaction is responsible for the magnetochiral effects in curved wires.

We consider three types of curvilinear uniaxial anisotropy which correspond to three possible curvilinear directions (1) (see Table I): (i) An easy-tangential anisotropy corresponds to the anisotropy axis $\boldsymbol{e}_\mathrm{an}$ directed along $\boldsymbol{e}_\mathrm{T}$, where the anisotropy interaction tries to orient the magnetization along the curve. Note that in soft magnets, such kind of anisotropy appears effectively as a shape anisotropy caused by the dipolar interaction [31]. (ii) An easy-normal anisotropy is determined

TABLE I. Types of equilibrium magnetization states for various uniaxial anisotropies in a helix-shaped magnetic wire. In Ref. [17] onion states were not observed.

		Magnetization states in a helix wire	
Anisotropy type	Anisotropy axis $\boldsymbol{e}_{an}$	Equilibrium states	Orientation according to Ref. [17]
Easy tangential	$\boldsymbol{e}_T$	Quasitangential state	Corkscrew
		Onion state	—
Easy normal	$\boldsymbol{e}_N$	Normal state	Radial
		Onion state	—
Easy binormal	$\boldsymbol{e}_B$	Quasibinormal state	Hollow bar
		Onion state	—

by the normal vector $\boldsymbol{e}_N$. (iii) An easy-binormal anisotropy direction corresponds to the binormal basic vector $\boldsymbol{e}_B$.

All three types of anisotropic magnets can be realized experimentally: In straight nanostrips/nanowires, the anisotropy can have well-defined uniaxial directions, e.g., in plane along the strip, in plane perpendicularly to the strip, or out of plane, which correspond to the uniformly magnetized samples in the corresponding direction. Using the coiling process [17], it is possible to obtain 3D microhelix coil strips with different magnetization orientation: corkscrew, radial, and hollow-bar magnetized (see Table I) to get a link between the anisotropy type and the magnetization orientation.

For the further analysis, it is convenient to introduce the angular parametrization of the magnetization unit vector $\boldsymbol{m}$ using the local Frenet-Serret reference frame,

$$\boldsymbol{m} = \sin\theta\cos\phi\,\boldsymbol{e}_T + \sin\theta\sin\phi\,\boldsymbol{e}_N + \cos\theta\,\boldsymbol{e}_B,$$

where the angular variables θ and ϕ depend on both spatial and temporal coordinates. Then the energy density (5) reads [11]

$$\begin{aligned}
\mathscr{E}_{ex} &= [\theta' - \tau\sin\phi]^2 + [\sin\theta(\phi' + \kappa) - \tau\cos\theta\cos\phi]^2,\\
\mathscr{E}_{an}^{ET} &= -\frac{\sin^2\theta\cos^2\phi}{w^2}, \quad \mathscr{E}_{an}^{EN} = -\frac{\sin^2\theta\sin^2\phi}{w^2}, \qquad (6)\\
\mathscr{E}_{an}^{EB} &= -\frac{\cos^2\theta}{w^2}.
\end{aligned}$$

Here, $\mathscr{E}_{an}^{ET}$, $\mathscr{E}_{an}^{EN}$, and $\mathscr{E}_{an}^{EB}$ denote anisotropy energy densities of easy-tangential, easy-normal, and easy-binormal types, respectively.

The magnetization dynamics follows the Landau-Lifshitz equation. In terms of the angular variables θ and ϕ, these equations read

$$\frac{M_s}{\gamma_0}\sin\theta\,\partial_t\phi = \frac{\delta E}{\delta\theta}, \quad -\frac{M_s}{\gamma_0}\sin\theta\,\partial_t\theta = \frac{\delta E}{\delta\phi}, \qquad (7)$$

with γ_0 being the gyromagnetic ratio.

III. EQUILIBRIUM MAGNETIZATION STATES OF A HELIX WIRE WITH EASY-TANGENTIAL ANISOTROPY

Hereafter we will be concerned with curvilinear effects in statics and dynamics of helical magnetic wires. A typical parametrization of the helix wire reads

$$\boldsymbol{\gamma}(\chi) = \hat{\boldsymbol{x}}R\cos\chi + \hat{\boldsymbol{y}}R\sin\chi + \hat{\boldsymbol{z}}p\chi, \qquad (8a)$$

where R is the helix radius, $p = P/(2\pi)$ with P being the pitch of the helix, and χ is the azimuthal angle of a cylindrical frame of reference with $\hat{\boldsymbol{z}}$ axis aligned along the helix axis; see Fig. 1. The helix has the constant curvature $\kappa = R/(R^2+p^2)$ and the torsion $\tau = p/(R^2+p^2)$. For the further analysis, it is instructive to rewrite (8a) as a function of the arc length s and in terms of the curvature and the torsion,

$$\begin{aligned}
\boldsymbol{\gamma}(s) &= \hat{\boldsymbol{x}}\kappa s_0^2\cos\left(\frac{s}{s_0}\right) + \hat{\boldsymbol{y}}\kappa s_0^2\sin\left(\frac{s}{s_0}\right) + \hat{\boldsymbol{z}}s_0\tau s,\\
s_0 &= \frac{1}{\sqrt{\kappa^2+\tau^2}}. \qquad (8b)
\end{aligned}$$

One has to notice a one-to-one correspondence between (R,p) and (κ,τ) parametrization; cf. (8a) and (8b).

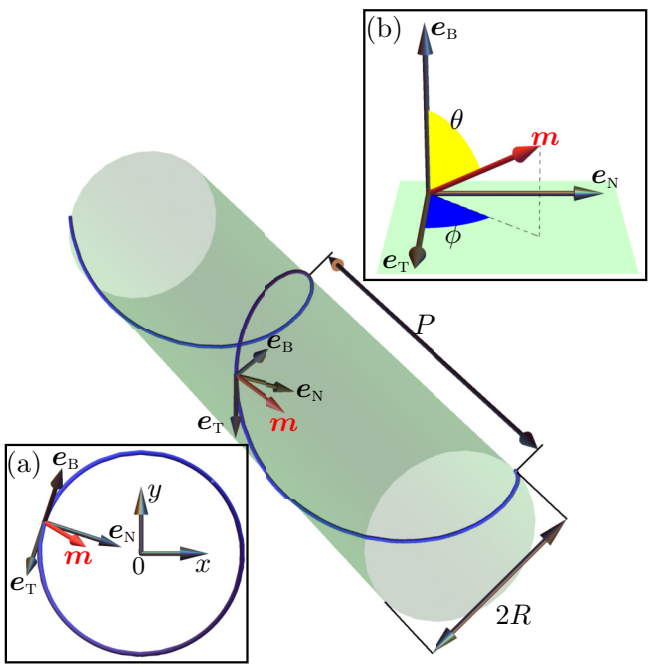

FIG. 1. (Color online) Schematics of the helix wire of the radius R and the pitch P. (a) Arrangement of the curvilinear Frenet-Serret reference frame $(\boldsymbol{e}_T,\boldsymbol{e}_N,\boldsymbol{e}_B)$ from the front view. (b) Arrangement of the magnetization angles θ and ϕ with respect to the magnetization unit vector $\boldsymbol{m}$.

By substituting the energy functional (6) into the Landau-Lifshitz equations (7), we get

$$
\begin{aligned}
&-\frac{M_s}{2\gamma_0\mathcal{A}}\sin\theta\,\partial_t\phi \\
&\quad=\tau\cos\phi(\kappa\cos 2\theta-2\partial_s\phi\sin^2\theta) \\
&\qquad+\partial_{ss}\theta-\sin\theta\cos\theta[(\kappa+\partial_s\phi)^2-\tau^2\cos^2\phi]-\frac{1}{2}\frac{\partial\mathscr{E}_{\rm an}}{\partial\theta}, \\
&\frac{M_s}{2\gamma_0\mathcal{A}}\sin\theta\,\partial_t\theta \\
&\quad=\sin\theta\cos\theta[2\partial_s\theta(\kappa+\partial_s\phi)-\kappa\tau\sin\phi] \\
&\qquad+\sin^2\theta[\partial_{ss}\phi+2\tau\partial_s\theta\cos\phi-\tau^2\sin\phi\cos\phi]-\frac{1}{2}\frac{\partial\mathscr{E}_{\rm an}}{\partial\phi},
\end{aligned}
\tag{9}
$$

where $\mathscr{E}_{\rm an}$ is the density of the anisotropy energy; see (6).

In this section, we are mostly interested in the case of easy-tangential anisotropy, which is typical for the wires. In this case, the anisotropy energy density has the form $\mathscr{E}_{\rm an}^{\rm ET}$; see (6).

First we discuss the limit case $\tau=0$ (ring wire instead of the helix). For any plane curve, the energy functional (6) with easy-tangential or easy-normal anisotropy is minimized by the plane magnetization distribution, $\theta_0=\pi/2$. The energy minimization with respect to ϕ results in the pendulum equation

$$\varkappa^2\partial_{\chi\chi}\phi-\sin\phi\cos\phi=0,\quad \varkappa=\kappa w,$$

with $\varkappa$ being a reduced curvature.

For relatively small values of the reduced curvature, $\varkappa<\varkappa_0\approx 0.657$, the equilibrium magnetization state of the ring is a homogeneous (in the curvilinear reference frame) vortex state $\phi^{\rm vor}$ and an inhomogeneous onion solution $\phi^{\rm on}$ for $\varkappa>\varkappa_0$ [11],

$$\phi^{\rm vor}=0,\pi,\quad \phi^{\rm on}=\frac{\pi}{2}-{\rm am}(x,k),\ x=\frac{2\chi}{\pi}{\rm K}(k). \tag{10}$$

Here, ${\rm am}(x,k)$ is the Jacobi amplitude [32] and the modulus k is determined by the condition

$$2\varkappa k{\rm K}(k)=\pi,$$

with ${\rm K}(k)$ being the complete elliptic integral of the first kind [32].

A. Quasitangential state

Now we consider the helix wire with a finite torsion, $\tau\neq 0$. Similar to the case of the ring wire, discussed above, we first look for the homogeneous (in the curvilinear reference frame) solution. This kind of solution is possible due to the constant curvature κ and the torsion τ. We can easily solve the static equations [see Eq. (9)] using the substitution $\theta(s)=\theta^t$ and $\phi(s)=\phi^t$:

$$\tan 2\theta^t=-\frac{2\mathcal{C}\sigma\varkappa}{1-\varkappa^2+\sigma^2},\quad \phi^t=0,\pi,$$

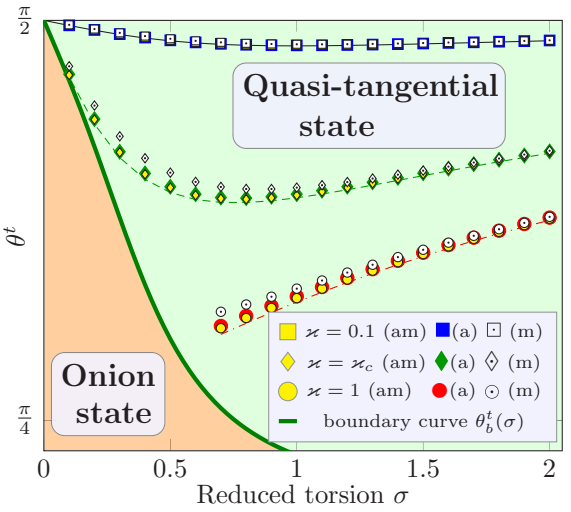

FIG. 2. (Color online) Equilibrium magnetization distribution in the quasitangential state of the helix wire with $\mathcal{C}=+1$. Lines correspond to the analytics; see Eq. (11). Symbols correspond to simulations: (a) anisotropic Heisenberg magnets [see (30)] ($Q=2$, $w=\ell$), (am) wires taking into account the dipolar interaction [see (29) and (32)] ($Q=2$, $w^{\rm eff}=2\ell/\sqrt{5}$), and (ms) isotropic wires taking into account the dipolar interaction [see (29) and (32)] ($Q=2$, $w^{\rm eff}=2\ell$). The boundary curve $\theta_b^t(\sigma)$ corresponds to (15).

where $\mathcal{C}=\cos\phi^t=\pm 1$, and the quantity $\sigma\equiv w\tau$ is a reduced torsion. Explicitly for the magnetization angles, we get

$$
\begin{aligned}
&\theta^t=\frac{\pi}{2}-\arctan\frac{2\mathcal{C}\sigma\varkappa}{V_0},\quad \phi^t=0,\pi, \\
&V_0=1+\sigma^2-\varkappa^2+V_1, \\
&V_1=\sqrt{(1-\varkappa^2+\sigma^2)^2+4\varkappa^2\sigma^2}.
\end{aligned}
\tag{11}
$$

The dependence $\theta^t(\varkappa,\sigma)$ is presented in Fig. 2.

In the limit case of very small curvature and torsion ($\varkappa,\sigma\ll 1$), the magnetization distribution becomes almost tangential [see Fig. 3(a)], with the asymptotic behavior

$$\theta^t\approx\frac{\pi}{2}-\mathcal{C}\sigma\varkappa\ \text{ for }\ \varkappa,\sigma\ll 1. \tag{12}$$

That is why we refer the state (11) as to the *quasitangential* state. Such a state is a finite torsion analog of the vortex state in the ring.

Even in the strong anisotropy case, the magnetization deviates from the tangential distribution: the inclination angle depends on the sign of $\mathcal{C}\sigma$. One can interpret the sign of σ as the helix chirality (different for a right-handed helix when $\sigma>0$ and left-handed one when $\sigma<0$); the quantity $\mathcal{C}$ can be interpreted as the magnetochirality, hence one can interpret it as a coupling between two chiralities.

The energy density (6) of the quasitangential state (11) reads

$$\mathscr{E}^t=-\frac{1-\varkappa^2-\sigma^2+V_1}{2w^2}.$$

It should be noted that the magnetization state in the helix nanowire was recently studied [33]: in particular, the magnon spectrum was shown to be affected by the curvature, which acts

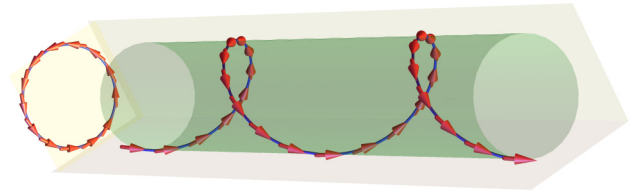

(a) Quasi-tangential state: $\varkappa = \sigma = 0.1$

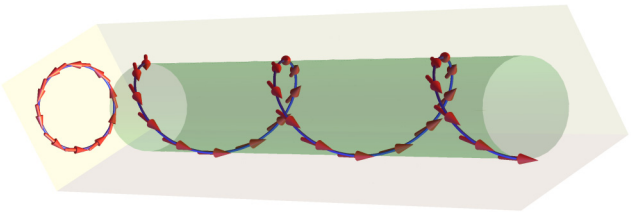

(b) Quasi-tangential state: $\varkappa = \sigma = \varkappa_0 \approx 0.657$

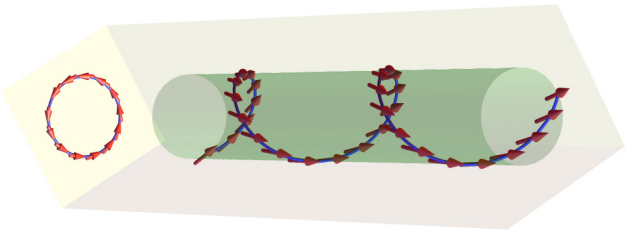

(c) Quasi-tangential state: $\varkappa = \sigma = 1$

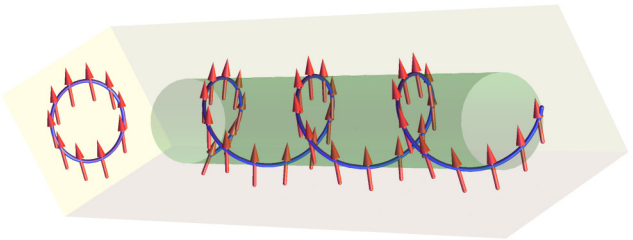

(d) Onion state: $\varkappa = 1.5$, $\sigma = 1$

FIG. 3. (Color online) Magnetization distributions in the helix wire with easy-tangential anisotropy and $\mathcal{C} = +1$ obtained from numerical simulations; see Sec. VI A.

mainly as an effective anisotropy. However, in Ref. [33], the equilibrium state was forcedly supposed to be the tangential one.

B. Onion state

Let us discuss the case of large curvature and torsion. We are looking for a solution that is periodic with respect to χ of the following form:

$$\theta^{\text{on}}(s) = \frac{\pi}{2} + \vartheta(\chi), \quad \phi^{\text{on}}(s) = -\chi + \varphi(\chi), \tag{13a}$$

with $\vartheta(\chi)$ and $\varphi(\chi)$ being 2π-periodic functions. In analogy with the ring wire ($\sigma = 0$) which possesses the exact onion solution (10), the magnetization distribution given by Eq. (13a) will be denoted as an *onion* solution.

Numerically, we found onion solutions for $\varkappa > \varkappa_0 \approx 0.657$ in a wide range of σ; see Figs. 3(c) and 4(a). The symmetry of the static form of Eqs. (9) dictates the symmetry of 2π-periodic functions ϑ and φ, which have the following Fourier expansion:

$$\vartheta(\chi) = \sum_{n=1}^{N} \vartheta_n \cos(2n-1)\chi, \quad \varphi(\chi) = \sum_{n=1}^{N} \varphi_n \sin 2n\chi, \tag{13b}$$

where $N \to \infty$. By substituting series (13b) into the static version of Eqs. (9), one can get a set of nonlinear equations for amplitudes ϑ_n and φ_n; see (A3). Finally, the energy of the onion state $\mathscr{E}^{\text{on}}(\sigma,\varkappa_b)$, averaged over the helix period, can be calculated numerically using amplitudes ϑ_n and φ_n; see the Appendix for details.

C. Phase diagram

Now we summarize the results of the equilibrium magnetization distribution. By comparing energies of different states, we find the energetically preferable states for different curvature and torsion values. The resulting phase diagram is presented in Fig. 4(a). There are two phases: (i) The quasitangential state is realized for relatively small curvatures, when $\varkappa < \varkappa_b(\sigma)$. In such a state, the magnetization direction is close to the direction of the easy-tangential anisotropy, $\boldsymbol{e}_{\text{T}}$; see Figs. 3(a) and 3(b). (ii) The onion state is energetically preferable, when $\varkappa > \varkappa_b(\sigma)$. The magnetization distribution is inhomogeneous in accordance with (13); see Fig. 3(d).

The boundary between two phases $\varkappa_b = \varkappa_b(\sigma)$ can be derived by using the condition

$$\mathscr{E}^{t}(\sigma,\varkappa_b) = \mathscr{E}^{\text{on}}(\sigma,\varkappa_b), \tag{14}$$

where $\mathscr{E}^{\text{on}}$ is the energy density of the onion state averaged over the helix period $2\pi s_0$; see (A4). We computed the boundary curve numerically for $N = 1$ and $N = 3$; see dot-dashed and solid lines, respectively, in Fig. 4(a). The two obtained curves are very close. The magnetization distribution in the onion state of the helix wire is spatially almost uniform; see Fig. 3(d).

For the approximate description of the boundary dependence, we use the trial function

$$\varkappa_b^{\text{ET}} = \sqrt{\varkappa_0^2 + 2\sigma^2},$$

which fits the numerically calculated curve $\varkappa_b(\sigma)$ with an accuracy of about 5×10^{-2}.

Using the boundary dependence $\varkappa_b(\sigma)$, one can easily compute the domain of applicability of the quasitangential solution (11),

$$\theta^t \in \begin{cases} \left(\theta_b^t, \frac{\pi}{2}\right) & \text{when } \mathcal{C}\sigma > 0, \\ \left(\frac{\pi}{2}, \theta_b^t\right) & \text{when } \mathcal{C}\sigma < 0. \end{cases} \tag{15}$$

Here, $\theta_b^t = \theta_b^t(\sigma)$ determines the boundary curve,

$$\theta_b^t(\sigma) \equiv \theta^t(\varkappa_b(\sigma),\sigma).$$

IV. SPIN-WAVE SPECTRUM IN A HELIX WIRE WITH EASY-TANGENTIAL ANISOTROPY

We limit our consideration of spin waves to the case of the quasitangential magnetization state. First we linearize the Landau-Lifshitz equations (9) on the background of the

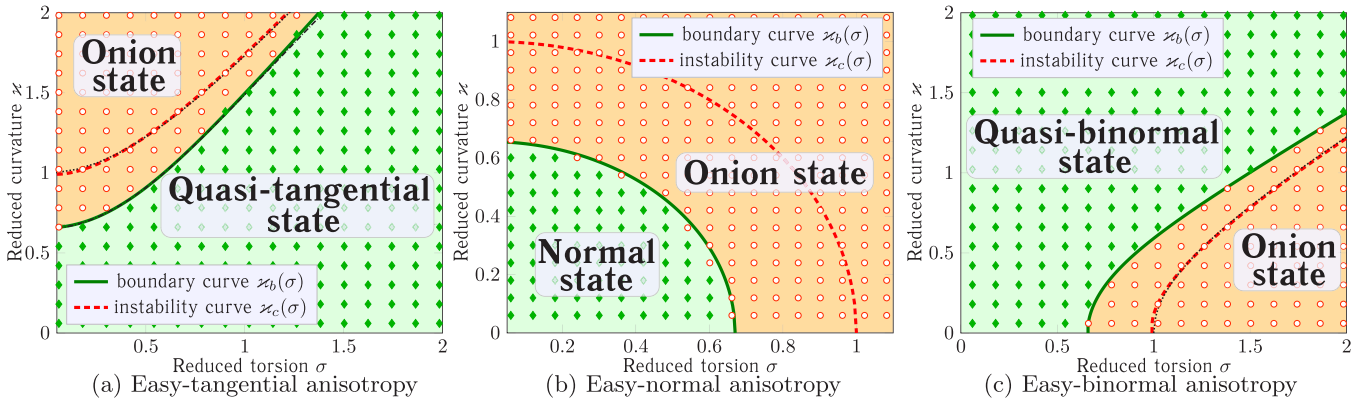

FIG. 4. (Color online) Phase diagram of equilibrium magnetization states for the helix wire with different types of anisotropy. Symbols correspond to simulation data: green diamonds to homogeneous (in curvilinear reference frame) states and open circles to the onion ones. (a) Easy-tangential case: the curve $\varkappa_b(\sigma)$ (solid green line), calculated by (14) with $N = 3$, describes the boundary between the quasitangential and the onion states; the dash-dotted line corresponds to $\varkappa_b(\sigma)$ with $N = 1$. The curve $\varkappa_c(\sigma)$ (dashed red line) describes the boundary of linear instability of the quasitangential state, and the dotted line is its fitting by (22). In the region between lines $\varkappa_b(\sigma)$ and $\varkappa_c(\sigma)$, the quasitangential state is metastable. (b), (c) Easy-normal and easy-binormal anisotropy, respectively; all notations have the same sense as in (a). Note that (b) has a different scale in order to show the normal-state region in detail.

quasitangential equilibrium state (11),

$$\theta(s,t) = \theta^t + \vartheta(s,t), \quad \phi(s,t) = \phi^t + \frac{\varphi(s,t)}{\sin\theta^t}.$$

Then, for ϑ and φ, we get the set of linear equations,

$$\partial_{t'}\varphi = -\partial_{\xi\xi}\vartheta + V_1\vartheta - 2A\partial_\xi\varphi,$$
$$-\partial_{t'}\vartheta = -\partial_{\xi\xi}\varphi + V_2\varphi + 2A\partial_\xi\vartheta,$$

where $\partial_{t'}$ is the derivative with respect to the dimensionless time $t' = \Omega_0 t$, with $\Omega_0 = 2K\gamma_0/M_s$, and ∂_ξ is the derivative with respect to the dimensionless coordinate $\xi = s/w$. Here, V_1 is determined according to (11), and the quantities V_2 and A have the following form:

$$V_2 = \frac{1+\varkappa^2+\sigma^2+V_1}{2},$$
$$A = -\varkappa\cos\theta^t - \sigma\mathcal{C}\sin\theta^t = -\sigma\mathcal{C}V_2\sqrt{\frac{2}{V_1V_0}}. \tag{16}$$

While V_1 and V_2 appear as scalar potentials, A acts as a vector potential $\boldsymbol{A} = A\boldsymbol{e}_\mathrm{T}$ of the effective magnetic field. This becomes obvious if we combine the set of linearized equations for ϑ and φ in a single equation for the complex-valued function $\psi = \vartheta + i\varphi$,

$$-i\partial_{t'}\psi = H\psi + W\psi^*, \quad H = (-i\partial_\xi - A)^2 + U. \tag{17a}$$

This differential equation has the form of a generalized Schrödinger equation, originally proposed for the description of spin waves on the magnetic vortex background [34]. The "potentials" in Eq. (17a) read

$$U = \frac{V_1+V_2}{2} - A^2, \quad W = \frac{V_1-V_2}{2} = -\frac{1+w^2\mathscr{E}^t}{2}. \tag{17b}$$

The vector potential $\boldsymbol{A}$ originates from the curvature-induced effective Dzyaloshinskii interaction; see Eq. (5). The harmonic part of the energy density $\mathscr{E}^\mathrm{D}_\mathrm{ex}$ in terms of the complex function ψ has a form [35]

$$\mathscr{E}^\mathrm{D}_\mathrm{ex} = -\frac{2}{w^2}A|\psi|^2\partial_\xi\arg\psi. \tag{18}$$

The spectrum of the spin waves of the helix wire is analyzed by considering the solutions of the linear system (17) of the form

$$\psi(\xi,t') = ue^{i\Phi} + ve^{-i\Phi}, \quad \Phi = q\xi - \Omega t' + \eta, \tag{19}$$

where $q = kw$ is a dimensionless wave number, $\Omega = \omega/\Omega_0$ is a dimensionless frequency, η is an arbitrary phase, and $u,v \in \mathbb{R}$ are constant amplitudes. The corresponding wave vector is oriented along the wire, $\boldsymbol{q} = q\boldsymbol{e}_\mathrm{T}$; its orientation with respect to the equilibrium magnetization is determined by Eq. (11). By substituting (19) into the generalized Schrödinger equation (17), one can obtain the eigenfrequency of the spin wave,

$$\Omega(q) = 2Aq + \sqrt{(q^2+V_1)(q^2+V_2)}. \tag{20}$$

Note that the dispersion of spin waves in the straight wire $\Omega_s(q) = 1 + q^2$ is mirror symmetric (i.e., it is invariant with respect to the transformation $q \to -q$) and has a gap [$\Omega_s(0) \neq 0$] which in dimensional units is proportional to the anisotropy constant $\Omega_0 \propto K$. In contrast, the magnon spectrum of the helix wire is not mirror symmetric, and has a gap at finite $q = q_0$; see Fig. 5. The gap $\Omega(q_0)$ depends both on the anisotropy constant and on the curvature and the torsion of the wire. The asymmetry in the dispersion law (20) is due to the presence of the effective Dzyaloshinskii interaction $\mathscr{E}^\mathrm{D}_\mathrm{ex}$.

In this context, it is instructive to mention that the spin-wave spectrum in the presence of Dzyaloshinskii-Moriya interaction is known to be asymmetric with respect to wave-vector inversion and has a minimum at finite wave vectors [25–27]. The curvature-induced asymmetry in the spin-wave propagation in nanotubes and its analogy with the Dzyaloshinskii-Moriya interaction was discussed recently in Ref. [36]. The spin-wave spectrum for the helix wire was calculated recently in Ref. [33]; however, the deviations from the pure tangential state were not

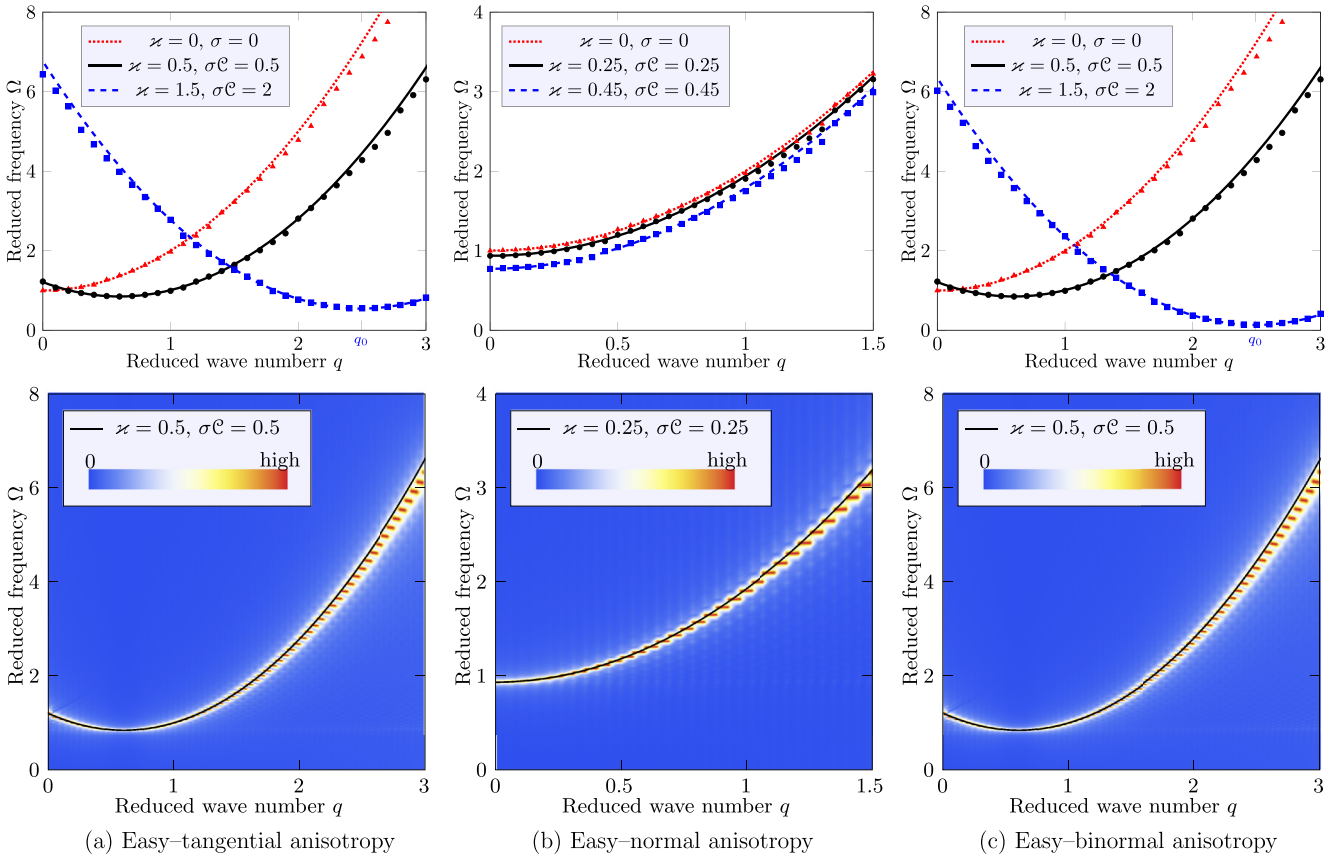

(a) Easy–tangential anisotropy (b) Easy–normal anisotropy (c) Easy–binormal anisotropy

FIG. 5. (Color online) The top row demonstrates dispersion laws for spin waves in the helix wire for different anisotropies. The equilibrium states are homogeneous in the curvilinear reference frame. The symbols correspond to simulation data (see Sec. VI B) and the lines correspond to the analytics; see Eqs. (20) and (26). A few examples of dispersion relation are shown at the bottom row in terms of density plots to demonstrate that (20) is a single-frequency branch in the system.

taken into account and the effective Dzyaloshinskii interaction was not considered.

In order to make some analytical estimates, we consider now the dispersion law for small curvatures and torsions,

$$\Omega(q) = \Omega_{\text{gap}} + (q - \mathcal{C}\sigma)^2 + \mathcal{O}(\varkappa^2,\sigma^2,\varkappa\sigma),$$

$$\Omega_{\text{gap}} = 1 - \frac{\varkappa^2}{2} + \mathcal{O}(\varkappa^2,\sigma^2,\varkappa\sigma).$$

One can see that the spin-wave spectrum asymmetry increases with increasing the torsion: the minimum of the frequency corresponds to $q_0 = \sigma\mathcal{C}$ (in dimensional units, the corresponding wave number $k_0 = \tau\mathcal{C}$) and its sign is determined by the product of the helix chirality and the magnetochirality.

A further increase of the curvature and torsion decreases the gap Ω_{gap}; there is a critical curve $\varkappa_c = \varkappa_c(\sigma)$, where the gap vanishes, $\Omega(q_c) = 0$ and $\partial_q\Omega(q_c) = 0$. One can easily find that $q_c = \mathcal{C}\sqrt{A^2 - U}$ and the critical curve $\varkappa_c = \varkappa_c(\sigma)$ can be found as a solution of the algebraic equation

$$4A^2U = W^2. \tag{21}$$

The critical curve $\varkappa_c(\sigma)$, calculated numerically, is plotted in Fig. 4(a) (dashed red curve). The trial function

$$\varkappa_c^{\text{trial}} = \sqrt{1 + 2\sigma^2} \tag{22}$$

fits the numerical results with an accuracy of about 5×10^{-3}; see the dotted curve in Fig. 4(a). In the region between the boundary curve $\varkappa_b(\sigma)$ and the instability curve $\varkappa_c(\sigma)$ (see Fig. 4), the quasitangential state becomes metastable.

V. HELIX WITH OTHER ANISOTROPY ORIENTATIONS

Let us discuss other types of anisotropies: easy normal and easy binormal; see Eqs. (6) and Table I.

A. Easy-normal anisotropy

Let us start the analysis of the easy-normal anisotropy with the limit case of the ring ($\tau = 0$). In this case, similarly to the easy-tangential anisotropy, the magnetization lies in the ring plane, $\theta = \pi/2$. The energy minimization with respect to ϕ results in the pendulum equation,

$$\varkappa^2\partial_{\chi\chi}\phi + \sin\phi\cos\phi = 0.$$

In analogy with the easy-tangential anisotropy case, the equilibrium state is the exactly normal state $\phi^n = \pm\pi/2$ for relatively small reduced curvatures $\varkappa < \varkappa_0$ and the onion state $\phi_n^{\text{on}}(\chi) = \pi/2 - \phi^{\text{on}}(\chi)$ for $\varkappa > \varkappa_0$, where function $\phi^{\text{on}}(\chi)$ is defined by Eq. (10).

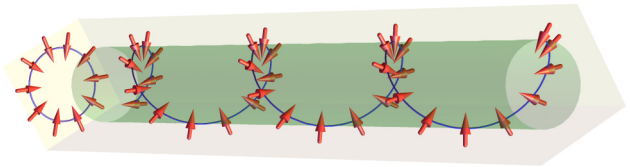

(a) Normal state: $\varkappa = \sigma = 0.45$

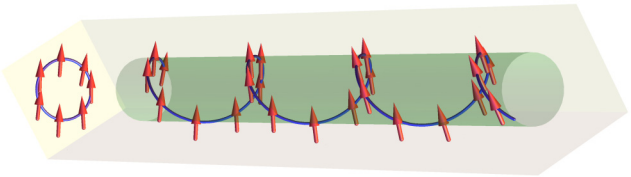

(b) Onion state: $\varkappa = \sigma = 1$

FIG. 6. (Color online) Magnetization distribution in the helix wire with $\mathcal{C} = +1$ and easy-normal anisotropy according to simulations data; see Sec. VI A.

In the case of finite torsion, there also exists *exactly normal* state

$$\theta^n = \frac{\pi}{2}, \quad \phi^n = \mathcal{C}\frac{\pi}{2}, \quad \mathscr{E}^n = -\frac{1-\varkappa^2-\sigma^2}{w^2}, \tag{23}$$

where $\mathcal{C} = \pm 1$; see Fig. 6(a). Such a state is energetically preferable for relatively small values of $\varkappa$ and σ. The magnetization in the normal state is directed exactly radially, which is well pronounced in experiments with 3D microhelix coil strips [17].

In the case of large curvature, there is the periodic (in curvilinear reference frame) onion solution, which has the form (13); see Fig. 6(b). Using the same numerical procedure as in Sec. III B, we evaluate the onion solution and compute the phase diagram; see Fig. 4(b).

For the approximate description of the boundary $\varkappa_b^{\mathrm{EN}}(\sigma)$ between two phases, we use the fitting function

$$\varkappa_b^{\mathrm{EN}} = \varkappa_0\sqrt{1-\left(\frac{\sigma}{\sigma_0}\right)^2}, \quad \sigma_0 \approx 0.67,$$

which fits the numerically calculated curve $\varkappa_b^{\mathrm{EN}}(\sigma)$ with an accuracy of about 3×10^{-3}.

Let us now discuss the linear excitations on the background of the normal solution. Using the same approach as in Sec. IV, we linearize Landau-Lifshitz equations (9) on the background of the normal solution (23), $\theta = \theta^n + \vartheta$, $\phi = \phi^n + \varphi$. As a result, one can get a generalized Schrödinger equation for the complex function $\psi = \vartheta + i\varphi$,

$$-i\partial_{t'}\psi = (-\partial_{\xi\xi} + U^n)\psi + W^n\psi^*.$$

Here the potentials read

$$U^n = 1 - \frac{\varkappa^2+\sigma^2}{2}, \quad W^n = \frac{1}{2}(\mathcal{C}\sigma - i\varkappa)^2. \tag{24}$$

Let us compare these equations with the generalized Schrödinger equation (17). First of all, there is no effective vector potential. The second difference is that the potential W^n in (24) is a complex-valued one; hence the scattering problem is similar to the two-channel scattering process. Similar to (19), we apply the following traveling-wave ansatz for the spin-wave complex magnon wave function:

$$\psi(\xi,t') = \psi_1 e^{i\Phi} + \psi_2 e^{-i\Phi}, \quad \Phi = q\xi - \Omega t' + \eta, \tag{25}$$

where $\psi_{1,2}$ are complex constant amplitudes, $\psi_{1,2} \in \mathbb{C}$. Now, by substituting the ansatz (25) into the generalized Schrödinger equation (24), one can derive the spectrum of the spin waves,

$$\Omega(q) = \sqrt{(1+q^2)(1+q^2-\varkappa^2-\sigma^2)}. \tag{26}$$

This dispersion relation is reproduced by the numerical simulations with a high accuracy; see Fig. 5(b). The critical dependence, where the gap of the spectrum vanishes, reads

$$\varkappa_c = \sqrt{1-\sigma^2};$$

see thick dashed curve in Fig. 5(b). In the region between the solid and dashed curves, the normal state is metastable.

The dispersion law (26) is symmetric with respect to the direction of the wave propagation: $\Omega(q) = \Omega(-q)$. Unlike the easy-tangential case, there is no effective magnetic field $\boldsymbol{A}$ because the curvature-induced effective Dzyaloshinskii interaction is absent in the harmonic approximation; cf. (18). The reason is that the equilibrium state is magnetized exactly in the normal direction $\boldsymbol{e}_{\mathrm{N}}$, which causes the degeneracy with respect to the sign of q. A similar behavior is known for thin films in the presence of Dzyaloshinskii-Moriya interaction, where the asymmetry in the spin-wave spectrum vanishes if the system is saturated perpendicularly to the film plane [26].

B. Easy-binormal anisotropy

If the anisotropy axis is directed along $\boldsymbol{e}_{\mathrm{B}}$, one has the easy-binormal anisotropy, $\mathscr{E}_{\mathrm{an}}^{\mathrm{EB}}$; see (6). The magnetization of the homogeneous (in the curvilinear reference frame) state reads

$$\tan 2\theta^b = \frac{2\mathcal{C}\varkappa\sigma}{1+\varkappa^2-\sigma^2}, \quad \cos\phi^b = \mathcal{C} = \pm 1. \tag{27}$$

Explicitly, θ^b reads

$$\theta^b = \frac{\pi}{2}[1+\mathrm{sgn}(\mathcal{C}\sigma)] - \arctan\frac{2\mathcal{C}\sigma\varkappa}{V_0^b},$$
$$V_0^b = 1+\varkappa^2-\sigma^2+V_1^b,$$
$$V_1^b = \sqrt{(1+\varkappa^2-\sigma^2)^2+4\varkappa^2\sigma^2}.$$

The magnetization of this state is close to the direction of the helix axis, and hence we name it a *quasibinormal* state; see Fig. 7(a). It corresponds to the hollow-bar magnetization distribution in the helix microcoils [17]. For different magnetization distributions, see also Table I.

The energy of the axial state reads

$$\mathscr{E}^b = -\frac{1-\varkappa^2-\sigma^2+V_1^b}{2w^2}.$$

Let us mention a formal analogy between the quasitangential state and the quasibinormal one: the energy of the quasitangential state can be obtained from the quasibinormal one by a replacement $\varkappa \leftrightarrow \sigma$.

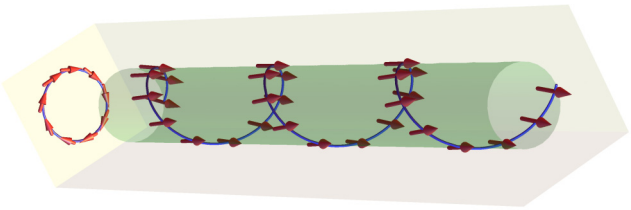

(a) Quasi-binormal state: $\varkappa = \sigma = 1.5$

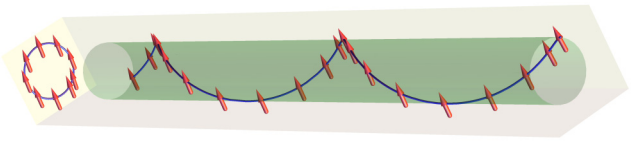

(b) Onion state: $\varkappa = 1$, $\sigma = 2$

FIG. 7. (Color online) Magnetization distribution in the helix wire with $\mathcal{C} = +1$ and easy-binormal anisotropy according to simulations data; see Sec. VI A.

The analogy between two states becomes more lucid if we use another parametrization for the magnetization $\boldsymbol{m}$,

$$\boldsymbol{m} = \cos\Theta\,\boldsymbol{e}_{\mathrm{T}} - \sin\Theta\sin\Phi\,\boldsymbol{e}_{\mathrm{N}} + \sin\Theta\cos\Phi\,\boldsymbol{e}_{\mathrm{B}},$$

where $\Theta = \Theta(s)$ and $\Phi = \Phi(s)$ are the angles in the Frenet-Serret frame of reference: The polar angle Θ describes the deviation of magnetization from the tangential curve direction, while the azimuthal angle Φ corresponds to the deviation from the binormal. Similar to (6), one can rewrite the energy terms as follows (cf. Appendix in Ref. [11] for details):

$$\mathscr{E}_{\mathrm{ex}} = [\Theta' - \kappa\sin\Phi]^2 + [\sin\Theta(\Phi' + \tau) - \kappa\cos\Theta\cos\Phi]^2,$$

$$\mathscr{E}_{\mathrm{an}}^{\mathrm{EB}} = -\frac{\sin^2\Theta\cos^2\Phi}{w^2}.$$

Now one can easily see that the energy functional of the easy-tangential magnet transforms to the energy functional of the easy-binormal magnet under the following conjugations: $\theta \to \Theta$, $\phi \to \Phi$, and $\varkappa \leftrightarrow \sigma$.

Similarly to the easy-tangential case, in the helix wire with the easy-binormal anisotropy there exist two equilibrium states: the homogeneous state (quasibinormal) and the periodic onion solution; see Fig. 7(b). The phase diagram, which separates these two states, is plotted in Fig. 4(c).

Now we discuss the magnons for the easy-binormal case. In analogy with the easy-tangential case, the linearized equations can be reduced to the generalized Schrödinger equation (17a) with the following potentials:

$$V_2^b = \frac{1 + \varkappa^2 + \sigma^2 + V_1^b}{2},$$

$$A^b = -\varkappa\cos\theta^b - \sigma\mathcal{C}\sin\theta^b = -\varkappa\mathcal{C}V_2^b\sqrt{\frac{2}{V_1^b V_0^b}}.$$

The dispersion law formally has the form (20) with the corresponding potentials described above. The dispersion curve is plotted in Fig. 5(c) for some typical parameters; it is confirmed by numerical simulations. The critical curve $\varkappa_c(\sigma)$, where the gap of the spectrum vanishes, can be found numerically using condition (21). The critical curve $\varkappa_c(\sigma)$, calculated numerically, is plotted in Fig. 4(c) (dashed red curve). For the approximate description of the critical dependence, we use the trial function

$$\varkappa_c^{\mathrm{trial}} = \sqrt{\frac{\sigma^2 - 1}{2}},$$

which fits the numerical results of Fig. 4(c) with an accuracy of about 2×10^{-2}; see the dotted curve in Fig. 4(c). In the region between solid and dashed curves, the quasibinormal state is metastable.

VI. SIMULATIONS

In order to verify our analytical results, we numerically simulate the magnetization dynamics of a helix-shaped chain of discrete magnetic moments $\boldsymbol{m}_i$ with $i = \overline{1,N}$. The shape of the chain is described by Eq. (8b). The magnetization dynamics of this system is determined by the set of Landau-Lifshitz equations,

$$\frac{1}{\omega_0}\frac{d\boldsymbol{m}_i}{dt} = \boldsymbol{m}_i \times \frac{\partial\mathcal{E}}{\partial\boldsymbol{m}_i} + \alpha\boldsymbol{m}_i \times \left[\boldsymbol{m}_i \times \frac{\partial\mathcal{E}}{\partial\boldsymbol{m}_i}\right], \tag{28}$$

where $\omega_0 = 4\pi\gamma_0 M_s$, α is the damping coefficient, and $\mathcal{E}$ is the dimensionless energy, normalized by $4\pi M_s^2 \Delta s^3$ with Δs being the sampling step of the natural parameter s. We consider four contributions to the energy of the system,

$$\mathcal{E} = \mathcal{E}^{\mathrm{ex}} + \mathcal{E}^{\mathrm{an}} + \mathcal{E}^{\mathrm{f}} + \mathcal{E}^{\mathrm{d}}. \tag{29a}$$

The first term in Eq. (29a) is the exchange energy,

$$\mathcal{E}^{\mathrm{ex}} = -2\frac{\ell^2}{\Delta s^2}\sum_{i=1}^{N-1}\boldsymbol{m}_i \cdot \boldsymbol{m}_{i+1},$$

with $\ell = \sqrt{A/(4\pi M_s^2)}$ being the exchange length. The second term determines the uniaxial anisotropy contribution,

$$\mathcal{E}^{\mathrm{an}} = -\frac{Q}{2}\sum_{i=1}^{N}\left(\boldsymbol{m}_i \cdot \boldsymbol{e}_i^{\mathrm{an}}\right)^2,$$

where $\boldsymbol{e}_i^{\mathrm{an}}$ is the coordinate-dependent unit vector along the anisotropy axis and Q is the quality factor; see (2). The third term determines the interaction with an external magnetic field $\boldsymbol{b}$,

$$\mathcal{E}^{\mathrm{f}} = -\sum_{i=1}^{N}\boldsymbol{b}_i \cdot \boldsymbol{m}_i,$$

where $\boldsymbol{b}_i$ is the dimensionless external field, normalized by $4\pi M_s$.

The last term in (29a) determines the dipolar interaction,

$$\mathcal{E}^{\mathrm{d}} = \frac{(\Delta s)^3}{8\pi}\sum_{i,j=1}^{N}{}' \frac{\boldsymbol{m}_i \cdot \boldsymbol{m}_j}{|\boldsymbol{r}_{ij}|^3} - 3\frac{(\boldsymbol{m}_i \cdot \boldsymbol{r}_{ij})(\boldsymbol{m}_j \cdot \boldsymbol{r}_{ij})}{|\boldsymbol{r}_{ij}|^5},$$

where $\boldsymbol{r}_{ij} \equiv \boldsymbol{\gamma}_i - \boldsymbol{\gamma}_j$.

The dynamical problem is considered as a set of $3N$ ordinary differential equations (28) with respect to $3N$ unknown functions $m_i^x(t)$, $m_i^y(t)$, $m_i^z(t)$ with $i = \overline{1,N}$. For given initial conditions, the set (28) is integrated numerically. During the integration process, the condition $|\boldsymbol{m}_i(t)| = 1$ is controlled.

We considered the helix wire with length $L = 500\Delta s$, the exchange length $\ell = 3\Delta s$, and the quality factor $Q = 2$ fixed. The curvature κ and the torsion τ were varied under the restriction $\Delta s \ll 2\pi/\sqrt{\kappa^2+\tau^2}$ (discretization step is much smaller than length of a single helix coil).

In most simulations, we neglect the magnetic dipolar interaction and consider the Heisenberg magnet with the energy

$$\mathcal{E}^{\mathrm{H}} = \mathcal{E}^{\mathrm{ex}} + \mathcal{E}^{\mathrm{an}} + \mathcal{E}^{\mathrm{f}}. \tag{30}$$

A. Equilibrium magnetization states

We start our simulations with easy-tangential magnets. In Sec. III A, we found that the curvature and the torsion cause the deviation of the magnetization from the anisotropy direction, which results in the magnetization distribution (11); such results are presented in Fig. 2 by the curves for three different value of the reduced curvature $\varkappa = 0.1, \varkappa_c, 1$ in the wide range of the torsion $\sigma \in (0;2)$. In order to verify our theoretical predictions, we simulate numerically Landau-Lifshitz equations (28) in the overdamped regime ($\alpha = 0.1$) during a long-time interval $\Delta t \gg (\alpha\omega_0)^{-1}$.

Numerically we model the anisotropic Heisenberg magnet with the energy (30) and $Q = 2$. Simulation data are presented in Fig. 2 by filled symbols and labeled as (a); one can see an excellent agreement between our theory and simulations. A typical magnetization distribution is shown in Figs. 3(a)–3(c) for the quasitangential states and in Fig. 3(d) for the onion state.

We also perform simulations for other anisotropy types. The magnetization distribution for the helix wire with easy-normal anisotropy is presented in Fig. 6(a) for the normal state and Fig. 6(b) for the onion one. For the case of easy-binormal anisotropy, one has two possible states: the quasibinormal one [see Fig. 7(a)] and the onion one [see Fig. 7(b)].

The second stage of our simulations is to find the equilibrium magnetization state of a given helix wire. Numerically, we simulate Eqs. (28) as described above for five different initial states, namely, the tangential, onion, normal, binormal, and random states. The final static state with the lowest energy is considered to be the equilibrium magnetization state. We obtain that for each type of anisotropy, the equilibrium state is either the onion state or anisotropy-aligned state (quasitangential, normal, and quasibinormal state for easy-tangential, easy-normal, and easy-binormal anisotropy, respectively). We present simulation data in Fig. 4 by symbols together with theoretical results (plotted by lines). One can see a very good agreement between simulations and analytics.

B. Dispersion relations

For each anisotropy-aligned equilibrium state, the magnon dispersion relation is obtained numerically. It is carried out in two steps. In the first step, the helix wire is relaxed in an external spatially nonuniform weak magnetic field,

$$\boldsymbol{b}_i^j = b_0 \boldsymbol{e}_i^{\mathrm{d}} \cos s_i k^j,$$

for a range of wave vectors $k^j = j/(300\Delta s)$ with $j = \overline{0,300}$. Here, $b_0 \ll 1$ is the field amplitude, and $s_i = (i-1)\Delta s$ is the position of the magnetic moment $\boldsymbol{m}_i$. The coordinate-dependent unit vector $\boldsymbol{e}_i^{\mathrm{d}}$ determines the magnetic field direction: $\boldsymbol{e}_i^{\mathrm{d}} = \boldsymbol{e}_{\mathrm{N}}$ for the quasitangential state and $\boldsymbol{e}_i^{\mathrm{d}} = \boldsymbol{e}_{\mathrm{T}}$ for normal and quasibinormal states.

In the second step, we switch off the magnetic field and simulate the magnetization dynamics with the damping value $\alpha = 0.01$ close to the natural one. Then the space-time Fourier transform is performed for one of the magnetization components (we consider the normal component for the quasitangential state and the tangential component for the other two equilibrium states). The frequency Ω which corresponds to the maximum of the Fourier signal is marked by a symbol for a given wave vector $q^j = wk^j$; see the top row of Fig. 5. The absence of additional peaks in the spectrum is demonstrated by the dispersion maps below; see bottom row of Fig. 5.

VII. DISCUSSION

We have performed a detailed study of statics and linear dynamics of magnetization in the helix wire with different anisotropy. We have limited our study by hard magnets, which can be well described by the model of anisotropic Heisenberg magnets. Our study was limited by the condition (3).

Let us discuss how our model can be generalized taking into account the long-range magnetostatics effects. The nonlocal magnetostatic interaction for thin wires of circular and square cross sections is known [31] to be completely reduced to a local effective easy-tangential anisotropy. It is important that such a conclusion survives for the case of curved wires [31]. Thus the magnetostatic interaction can be taken into account as an additional anisotropy. In general, one has to consider the model of a biaxial magnet. Here we limit ourselves by the helix wire with easy-tangential magnetocrystalline anisotropy. In this case, the magnetostatics effects can be taken into account by a simple redefinition of the anisotropy constants, leading to a new magnetic length,

$$\begin{aligned} K &\to K^{\mathrm{eff}} = K + \pi M_s^2, \\ w &\to w^{\mathrm{eff}} = \sqrt{\frac{A}{K^{\mathrm{eff}}}} = \frac{2\ell}{\sqrt{1+2Q}}. \end{aligned} \tag{31}$$

Thus our model (4) is also suitable for thin wires made of a magnetically *soft* material under the restriction

$$h \ll w,\ \ell,\ \frac{1}{\kappa},\ \frac{1}{\tau}.$$

In order to check our predictions about the effective anisotropy, we perform numerical simulations taking into account the nonlocal dipolar interaction as described in Sec. VI. Numerically, we integrate Eqs. (28) with the energy (29).

First, we simulate the anisotropic wire taking into account the dipolar interaction with the energy (29). In this case, we need to modify the magnetic length according to (31). Thus we also need to redefine the reduced curvature and torsion as follows:

$$\varkappa \to \varkappa^{\mathrm{eff}} = \tau w^{\mathrm{eff}}, \quad \sigma \to \sigma^{\mathrm{eff}} = \tau w^{\mathrm{eff}}. \tag{32}$$

For the case $Q = 2$, one gets $\ell = w$ and $w^{\mathrm{eff}} = 2\ell/\sqrt{5}$. One can see that we have a very nice agreement between the analytical results (11) and simulations data; see yellow symbols in Fig. 2. We label these data as (am).

The second kind of simulations taking into account the dipolar interaction was aimed to verify the validity of our approach for *soft* magnets with $Q = 0$. For this purpose, we model the soft isotropic wire taking into account the dipolar interaction. According to (31), we get $w^{\rm eff} = 2\ell$. Simulation data are presented in Fig. 2 by dotted symbols [labeled as (m)] for the curvature and the torsion redefined according to (32). By comparing the simulation data with analytical results, one can see a pretty good agreement in the wide range of curvatures and torsions. Our simulation data for soft magnets differ from the theoretical predictions for hard magnets only for relatively large values of the curvature in the vicinity of the boundary which separates the quasitangential state and the onion state.

Thus we can conclude that our model of the anisotropic Heisenberg magnet is physically sound also for thin wires made of a magnetically soft material.

In conclusion, we have presented a detailed study of statics and linear dynamics of magnetization in the helix wire. We have described equilibrium magnetization states for three types of uniaxial anisotropy, according to possible curvilinear directions. All three cases have been realized experimentally in rolled-up ferromagnetic microhelix coils [17]. We have calculated the phase diagram of possible states in the case of easy-tangential anisotropy: the quasitangential configuration (11) is energetically preferable for the strong anisotropy case. In this case, the deviations from the strictly tangential direction (corkscrew orientation [17]) are caused by the torsion, and the direction of the deviation depends on both helix chirality and the magnetochirality of the magnetization structure; see Eq. (12). In helix wires with large curvature, the equilibrium state is the onion state (13). The same situation is observed in magnetic ring wires [37,38]. The magnetization distribution (27) of the quasibinormal state is directed almost along the binormal (hollow-bar) orientation [17]. In contrast to the quasitangential state and quasibinormal one (which are realized for the easy-tangential and easy-binormal magnets, respectively), the normal state for the easy-normal magnets has several peculiarities: (i) The magnetization of the wire is *strictly* parallel to the normal direction $\boldsymbol{e}_{\rm N}$; see (23). (ii) The normal-state phase is realized for small curvatures and torsions only: $\varkappa^2/\varkappa_0^2 + \sigma^2/\sigma_0^2 < 1$; see Fig. 4(b). (iii) The spectrum of spin waves on the normal-state background is symmetric with respect to the direction of the wave propagation.

The torsion of the wire manifests itself in the magnetization dynamics: an effective magnetic field, induced by the torsion, breaks the mirror symmetry with the spin-wave direction. The dispersion law of spin waves (20) is essentially affected by this field.

There is a connection between the helix geometry and the tube one: when the helix pitch vanishes, we have a close-coiled solenoid magnet with properties similar to the thin-shell nanotube. The spin-wave spectrum in the nanotube is known [39] to have a gap, caused by the curvature. This conclusion is in agreement with the dispersion law for the helix wire; see Fig. 5(a). One has to note that the analogy between two systems is adequate under the restriction of vanishing torsions ($\sigma \to 0$); this explains the absence of the linear shift in the dispersion law for the nanotube in comparison with (20). In general, the transition from 1D to 2D systems requires a more accurate account of the dipolar interaction.

We considered the simplest example of the curved wire with constant curvature and torsion. Our results can be generalized for the case of variables parameters $\kappa(s)$ and $\tau(s)$. To summarize, we can formulate a few general remarks about the curvature and torsion effects in the spin-wave dynamics. The linear magnetization dynamics can be described by the generalized Schrödinger equation (17). In the case of the straight wire, one has the standard Schrödinger equation for the complex magnon wave function ψ with a typical potential scattering. The curvature induces an additional effective potential: the "geometrical potential" [29]. This is described by the modification of effective potential U in Eq. (17b). Besides, there is a curvature-induced coupling potential W: the problem becomes different in principle from the usual set of coupled Schrödinger equations; see the discussion in Ref. [34]. Due to the torsion influence, there appears an effective magnetic field. The vector potential of this field is constant for the helix wire [see (16)], and hence the effective magnetic flux density $\boldsymbol{B} = \nabla \times \boldsymbol{A}$ vanishes. Nevertheless, the presence of magnetic field with the vector potential $\boldsymbol{A}$ breaks the mirror symmetry of the problem: the motion of magnetic excitations in different spatial direction is not identical.

Let us mention the connection between the vector potential and the effective Dzyaloshinskii interaction: the total energy of the Dzyaloshinskii interaction $\mathscr{E}_{\rm ex}^{\rm D} \propto \int ds\, \boldsymbol{A}\cdot\boldsymbol{j}$ with the current $\boldsymbol{j} = |\psi|^2 \nabla \arg\psi$; see Eq. (18). Using the explicit form of the integrand, one can find that $\mathscr{E}_{\rm ex}^{\rm D} \propto \sigma q \mathcal{C}$. This expression shows a relation between the topology of the wire (namely, helix chirality) with the topology of the magnetic structure (namely, the magnetochirality). In this context, it is instructive to note that there is a deep analogy between the Dzyaloshinskii-Moriya interaction and the Berry phase theory [40].

We expect that our approach can be easily generalized for the arbitrary curved wires, where all potentials becomes spatially dependent: $U(s)$, $W(s)$, and $A(s)$. Depending on the curvature and the torsion, these potentials can repel or attract magnons. In the latter case, there can appear a well with possible bound states, i.e., local modes.

ACKNOWLEDGMENTS

The authors thank D. Makarov for stimulating discussions and acknowledge the IFW Dresden, where part of this work was performed, for kind hospitality. D.D.S. thanks F. G. Mertens for helpful discussions and the University of Bayreuth, where part of this work was performed, for kind hospitality, and also acknowledges the support from the Alexander von Humboldt Foundation. The present work was supported by the Program of Fundamental Research of the Department of Physics and Astronomy of the National Academy of Sciences of Ukraine (Project No. 0112U000056).

APPENDIX: ONION-STATE SOLUTION

We start from the static form of the Landau-Lifshitz equations (9),

$$F(\theta,\phi) = 0, \quad G(\theta,\phi) = 0, \tag{A1}$$

with F and G being the nonlinear operators,

$$\begin{aligned} F(\theta,\phi) =& -\partial_{\chi\chi}\theta - \sigma\cos\phi(\varkappa\cos 2\theta - 2\partial_\chi\phi\sin^2\theta) \\ &+ \sin\theta\cos\theta[(\varkappa+\partial_\chi\phi)^2 - (1+\sigma^2)\cos^2\phi], \\ G(\theta,\phi) =& \sin^2\theta[-\partial_{\chi\chi}\phi + (1+\sigma^2)\sin\phi\cos\phi. \\ &- 2\sigma\partial_\chi\theta\cos\phi] + \sin\theta\cos\theta[\varkappa\sigma\sin\phi \\ &- 2\partial_\chi\theta(\varkappa+\partial_\chi\phi)]. \end{aligned}$$

By substituting here the expansion (13) in the form

$$\begin{aligned} \theta(\chi) &= \frac{\pi}{2} + \varepsilon\sum_{n=1}^{N}\vartheta_n\cos(2n-1)\chi, \\ \phi(\chi) &= -\chi + \varepsilon\sum_{n=1}^{N}\varphi_n\sin 2n\chi, \end{aligned} \tag{A2}$$

and expanding results into series over ε up to the Nth order, one can get the Fourier expansion of operators F and G as follows:

$$\begin{aligned} F(\theta,\phi) &= \sum_{n=1}^{N} F_n(\vartheta_1,\ldots,\vartheta_n;\varphi_1,\ldots,\varphi_n)\cos(2n-1)\chi, \\ G(\theta,\phi) &= \sum_{n=1}^{N} G_n(\vartheta_1,\ldots,\vartheta_n;\varphi_1,\ldots,\varphi_n)\sin 2n\chi. \end{aligned}$$

Here, F_n and G_n are polynomials of the order n with respect to ϑ_k and φ_k. Then the Landau-Lifshitz equations (A1) result in the set of nonlinear polynomial equations,

$$\begin{aligned} &F_n(\vartheta_1,\ldots,\vartheta_n;\varphi_1,\ldots,\varphi_n) = 0 \\ &G_n(\vartheta_1,\ldots,\vartheta_n;\varphi_1,\ldots,\varphi_n) = 0, \end{aligned} \qquad n = \overline{1,N}, \tag{A3}$$

which can be solved numerically on ϑ_k and φ_k with any precision.

In order to calculate the energy of the onion state, we substitute the magnetization angles θ and ϕ in the form (A2) into the energy density (6), expand the results over ε up to the $2N$th order, and average the result over the helix period,

$$\begin{aligned} \mathscr{E}^{\text{on}}(\sigma,\varkappa) &= \frac{1}{2\pi}\int_0^{2\pi}\mathscr{E}d\chi, \\ \mathscr{E} &= \mathscr{E}_{\text{ex}} + \mathscr{E}_{\text{an}}^{\text{ET}} = \mathscr{E}(\vartheta_1,\ldots,\vartheta_n;\varphi_1,\ldots,\varphi_n). \end{aligned} \tag{A4}$$

[1] D. Makarov, C. Ortix, and L. Baraban, Guest editorial—functional magnetic nanomembrane, SPIN **3**, 1302001 (2013).

[2] A. Saxena, R. Dandoloff, and T. Lookman, Deformable curved magnetic surfaces, Physica A **261**, 13 (1998).

[3] V. L. Carvalho-Santos and R. Dandoloff, Topological spin excitations induced by an external magnetic field coupled to a surface with rotational symmetry, Brazil. J. Phys. **43**, 130 (2013).

[4] V. L. Carvalho-Santos, A. R. Moura, W. A. Moura-Melo, and A. R. Pereira, Topological spin excitations on a rigid torus, Phys. Rev. B **77**, 134450 (2008).

[5] M.-W. Yoo and S.-K. Kim, Curved geometrical confinement effect on vortex-state reversals in magnetic half-spheres, Appl. Phys. Express **8**, 063003 (2015).

[6] V. P. Kravchuk, D. D. Sheka, R. Streubel, D. Makarov, O. G. Schmidt, and Y. Gaididei, Out-of-surface vortices in spherical shells, Phys. Rev. B **85**, 144433 (2012).

[7] R. Streubel, V. P. Kravchuk, D. D. Sheka, D. Makarov, F. Kronast, O. G. Schmidt, and Y. Gaididei, Equilibrium magnetic states in individual hemispherical permalloy caps, Appl. Phys. Lett. **101**, 132419 (2012).

[8] D. D. Sheka, V. P. Kravchuk, M. I. Sloika, and Y. Gaididei, Equilibrium states of soft magnetic hemispherical shell, SPIN **3**, 1340003 (2013).

[9] R. Streubel, D. J. Thurmer, D. Makarov, F. Kronast, T. Kosub, V. Kravchuk, D. D. Sheka, Y. Gaididei, R. Schaefer, and O. G. Schmidt, Magnetically capped rolled-up nanomembranes, Nano Lett. **12**, 3961 (2012).

[10] Y. Gaididei, V. P. Kravchuk, and D. D. Sheka, Curvature Effects in Thin Magnetic Shells, Phys. Rev. Lett. **112**, 257203 (2014).

[11] D. D. Sheka, V. P. Kravchuk, and Y. Gaididei, Curvature effects in statics and dynamics of low dimensional magnets, J. Phys. A: Math. Theor. **48**, 125202 (2015).

[12] V. L. Carvalho-Santos, R. G. Elias, J. M. Fonseca, and D. Altbir, Curvature-induced changes in the magnetic energy of vortices and skyrmions in paraboloidal nanoparticles, J. Appl. Phys. **117**, 17E518 (2015).

[13] P. Landeros and Álvaro S. Núñez, Domain wall motion on magnetic nanotubes, J. Appl. Phys. **108**, 033917 (2010).

[14] J. Otálora, J. A. López-López, P. Vargas, and P. Landeros, Chirality switching and propagation control of a vortex domain wall in ferromagnetic nanotubes, Appl. Phys. Lett. **100**, 072407 (2012).

[15] M. Yan, C. Andreas, A. Kakay, F. Garcia-Sanchez, and R. Hertel, Chiral symmetry breaking and pair-creation mediated Walker breakdown in magnetic nanotubes, Appl. Phys. Lett. **100**, 252401 (2012).

[16] O. V. Pylypovskyi, V. P. Kravchuk, D. D. Sheka, D. Makarov, O. G. Schmidt, and Y. Gaididei, Coupling of Chiralities in Spin and Physical Spaces: The Möbius Ring as a Case Study, Phys. Rev. Lett. **114**, 197204 (2015).

[17] E. J. Smith, D. Makarov, S. Sanchez, V. M. Fomin, and O. G. Schmidt, Magnetic microhelix coil structures, Phys. Rev. Lett. **107**, 097204 (2011).

[18] E. J. Smith, D. Makarov, and O. G. Schmidt, Polymer delamination: towards unique three-dimensional microstructures, Soft Matter **7**, 11309 (2011).

[19] R. Streubel, J. Lee, D. Makarov, M.-Y. Im, D. Karnaushenko, L. Han, R. Schäfer, P. Fischer, S.-K. Kim, and O. G. Schmidt, Magnetic microstructure of rolled-up single-layer ferromagnetic nanomembranes, Adv. Mater. **26**, 316 (2014).

[20] I. Mönch, D. Makarov, R. Koseva, L. Baraban, D. Karnaushenko, C. Kaiser, K.-F. Arndt, and O. G. Schmidt, Rolled-up magnetic sensor: Nanomembrane architecture for in-flow detection of magnetic object, ACS Nano **5**, 7436 (2011).

[21] F. Balhorn, S. Mansfeld, A. Krohn, J. Topp, W. Hansen, D. Heitmann, and S. Mendach, Spin-Wave Interference in Three-Dimensional Rolled-Up Ferromagnetic Microtubes, Phys. Rev. Lett. **104**, 037205 (2010).

[22] F. Balhorn, C. Bausch, S. Jeni, W. Hansen, D. Heitmann, and S. Mendach, Azimuthal spin-wave modes in rolled-up permalloy microtubes: Tuneable mode frequency, mode patterns, and mode splitting, Phys. Rev. B **88**, 054402 (2013).

[23] A. A. Solovev, S. Sanchez, M. Pumera, Y. F. Mei, and O. G. Schmidt, Magnetic control of tubular catalytic microbots for the transport, assembly, and delivery of micro-object, Adv. Funct. Mater. **20**, 2430 (2010).

[24] K. E. Peyer, S. Tottori, F. Qiu, L. Zhang, and B. J. Nelson, Magnetic helical micromachines, Chem. Eur. J. **19**, 28 (2012).

[25] K. Zakeri, Y. Zhang, J. Prokop, T.-H. Chuang, N. Sakr, W. X. Tang, and J. Kirschner, Asymmetric spin-wave dispersion on Fe(110): Direct evidence of the Dzyaloshinskii-Moriya interaction, Phys. Rev. Lett. **104**, 137203 (2010).

[26] D. Cortes-Ortuno and P. Landeros, Influence of the Dzyaloshinskii-Moriya interaction on the spin-wave spectra of thin films, J. Phys.: Condens. Matter **25**, 156001 (2013).

[27] K. Zakeri, Elementary spin excitations in ultrathin itinerant magnets, Phys. Rep. **545**, 47 (2014).

[28] A. Hubert and R. Schäfer, *Magnetic Domains: The Analysis of Magnetic Microstructures* (Springer-Verlag, Berlin, 1998).

[29] R. C. T. da Costa, Quantum mechanics of a constrained particle, Phys. Rev. A **23**, 1982 (1981).

[30] V. S. Tkachenko, A. N. Kuchko, M. Dvornik, and V. V. Kruglyak, Propagation and scattering of spin waves in curved magnonic waveguides, Appl. Phys. Lett. **101**, 152402 (2012).

[31] V. V. Slastikov and C. Sonnenberg, Reduced models for ferromagnetic nanowires, IMA J. Appl. Math. **77**, 220 (2012).

[32] *NIST Handbook of Mathematical Functions*, edited by F. W. J. Olver, D. W. Lozier, R. F. Boisvert, and C. W. Clark (Cambridge University Press, New York, 2010).

[33] V. S. Tkachenko, A. N. Kuchko, and V. V. Kruglyak, An effect of the curvature induced anisotropy on the spectrum of spin waves in a curved magnetic nanowire, Low Temp. Phys. **39**, 163 (2013).

[34] D. D. Sheka, I. A. Yastremsky, B. A. Ivanov, G. M. Wysin, and F. G. Mertens, Amplitudes for magnon scattering by vortices in two–dimensional weakly easy–plane ferromagnets, Phys. Rev. B **69**, 054429 (2004).

[35] Up to a full derivative with respect to ξ.

[36] R. Hertel, Curvature–induced magnetochirality, SPIN **03**, 1340009 (2013).

[37] M. Kläui, C. A. F. Vaz, L. Lopez-Diaz, and J. A. C. Bland, Vortex formation in narrow ferromagnetic rings, J. Phys.: Condens. Matter **15**, R985 (2003).

[38] A. P. Guimarães, *Principles of Nanomagnetism*, *NanoScience and Technology* (Springer-Verlag, Berlin Heidelberg, 2009).

[39] A. González, P. Landeros, and Álvaro S. Núñez, Spin wave spectrum of magnetic nanotubes, J. Magn. Magn. Mater. **322**, 530 (2010).

[40] F. Freimuth, S. Blügel, and Y. Mokrousov, Berry phase theory of Dzyaloshinskii–Moriya interaction and spin–orbit torques, J. Phys.: Condens. Matter **26**, 104202 (2014).